A Design for a Precision 10-m Sub-Millimeter Antenna

David P. Woody and James W. Lamb

***Abstract*— This paper presents a telescope design that should meet the stringent specifications for the Millimeter Array antennas. The most critical specifications are 25 μm surface accuracy, 0.8 arcsec pointing precision, and the ability to switch between two source separated by 1.5° in less than 1.5 s. The major design concepts employed to attain the required performance for a 10-m diameter antenna are a spaceframe backup structure supported at a radius of 3.3 m, a wide base mount with a wheel and track azimuth bearing, low thermal expansion materials, and an independent pointing reference structure.**

I. Introduction

The National Radio Astronomy Observatory (NRAO) is in the process of designing and developing the components for a Millimeter Array (MMA) which will consist of upward of 50 antennas located on a 5,000 m altitude site in the Atacama desert in Chile. The science goals range from detection of the weakest sources at frequencies as high as 950 GHz to imaging wide fields with good fidelity and high dynamic range at 300 GHz. These goals demand that the antennas perform significantly better than the current generation of millimeter and sub-millimeter telescopes.

The baseline design is for 10-m diameter telescopes with conventional Cassegrain optics, but with very exacting performance specifications. The most demanding specifications are the wave front error, pointing accuracy and fast position switching capability. The wave front error should correspond to an effective surface error of less than 25 μm RMS. The telescope must point with an accuracy of better than 0.8 arcsec RMS. It must also be able to slew to a new position 1.5° away and settle to within 3 arcsec in less than 1.5 s. These specifications must be met under most day and night conditions at the high altitude site in Chile.

The high surface accuracy is driven by the need to image wide fields at 1-mm wavelength as well as the need for high aperture efficiency at 0.3-mm wavelength. These same goals also drive the 0.8 arcsec pointing requirement. The fast position switching will allow for a very fast cycle time between observations of the target source and a nearby phase calibrator, allowing removal of a large part of the phase errors caused by fluctuations in the atmosphere.

This paper describes an antenna design concept to meet the stringent MMA specifications at an affordable cost. The design uses features that have been proven to work in existing telescopes and draws upon ideas proposed by other millimeter antenna designers. The innovative concepts presented by Dietmar Plathner have been particularly important in inspiring us in the direction this design has taken [1].

The proposed telescope design is shown in Figure 1. The primary and secondary reflectors and elevation tipping structure are described in the next section. Section III describes the mount including the rotating azimuth structure with a wheel and track azimuth bearing. The independent pointing reference system is described in section IV. A possible transporter configuration in presented in Section V.

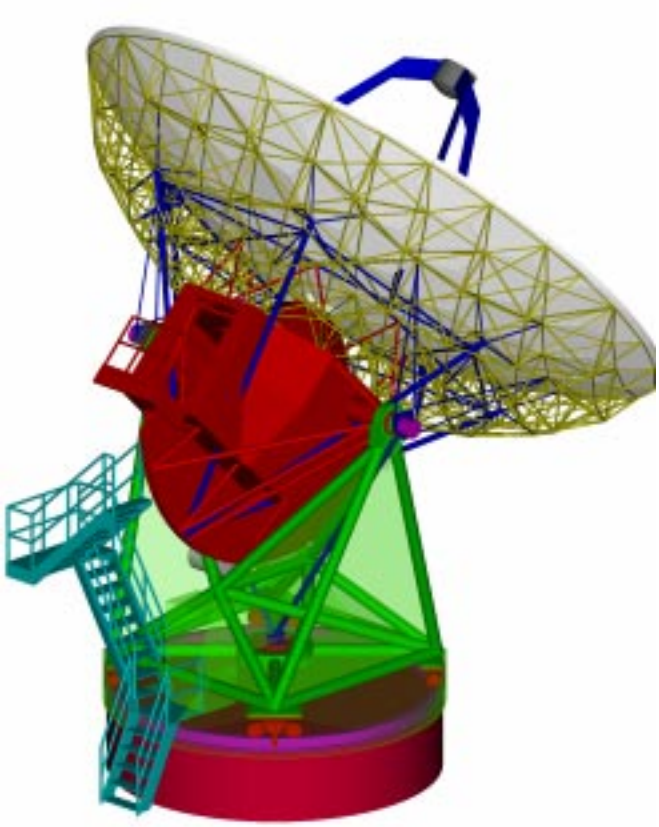

Fig. 1. Rendering of 10.4-m telescope design. The steel base and elevation tipping structure are shown in red. The CFRP feedlegs, BUS support and pointing reference structure are shown in blue. The CFRP BUS is yellow. The azimuth rotating structure is green and is translucent to reveal the pintle bearing and pointing reference structure. The azimuth track is purple.

10 March, 1999.

Owens Valley Radio Observatory, California Institute of Technology, Big Pine, CA 93513, USA

Section VI presents the results of the finite element analyses that have been carried out for this design with the design concepts and performance summarized in section VII.

II. Reflector and Tipping Structure

Meeting the diverse and exacting set of specifications for the MMA telescopes, including the high surface precision in most weather conditions, high pointing accuracy and fast position switching, will require a very stiff structure. Although homology has proven to be a very successful technique for reducing the gravitational distortions in large antennas [2], [3], [4], optimizing the homology of a structure tends to make it less stiff and hence may degrade its performance under variable wind loads. The basic approach taken in the design presented here is to build a very rigid structure to meet the pointing and surface error specifications and not require a high degree of homology to keep the gravitational deformations within the error budget. This has the advantage of not requiring the tight control of construction material parameters necessary for highly homologous designs.

A. Backup Structure and Optimum Support Radius

The typical radio telescope supports the backup structure (BUS) and reflector assembly from a relatively small hub at the reflector vertex. The stiffness can be increased dramatically by using a ring of support points at a much larger radius.

Analytical formulas have been derived for the gravitational distortions for a uniform disk support on a ring [5]. The classical result is that the peak-to-peak distortions are minimized for support at a radius of 0.679 of the disk radius. Fig. 2 shows the RMS distortion for a 1 m thick 10 m diameter disk as a function of the support radius. The density, Young's modulus, and Poisson's ratio were chosen to simulate a steel spaceframe with an average filling fraction of 1%. The RMS distortion has a sharp minimum at 3.41 m, almost identical to the radius of support that minimizes the peak-to-peak distortions. The RMS distortions double for a change of only 5% in the radius of the support ring. The uniform disk is 20 times stiffer when supported at this radius compared to support at a radius of 1.6 m.

We can extend these calculations by calculating the deviations from homology. Fig. 2 shows the RMS residual after removing a best-fit paraboloid from the distortions. At small support radii, the RMS error decreases by a factor of five. The minimum in the RMS homology residual is at 2.82 m corresponding to 0.564 of the disk radius. The ratio of the RMS before and after removing the best-fit paraboloid is 15 at this optimum homology point. The minimum RMS distortion without using homology at 0.682 of the disk radius is only twice the homology optimum. Thus supporting a uniform disk on ring at a radius somewhere between 0.56 and 0.68 of the disk radius will minimize the gravitational distortions.

We have verified that this conclusion also holds for the modified version of the Leighton BUS [3] proposed here. In

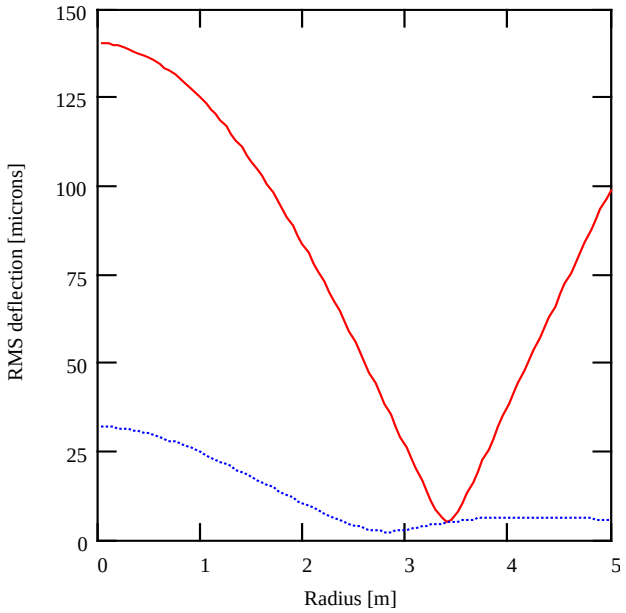

Fig. 2. Plot of the RMS distortions of a 1 m thick 10 m diameter uniform disk as a function of the radius of the support ring. Solid red line is the RMS distortion without fitting while the dashed blue line is the RMS deviations after removing the best-fit paraboloid.

plan view, the top and bottom layers of struts and nodes form a uniform equilateral triangular grid with a grid spacing of 1/9 of the reflector diameter. Struts parallel to the optical axis plus diagonal members connect the top and bottom nodes. The innermost bottom three nodes from the Leighton design were eliminated to increase the available volume near the vertex for receivers. In addition, the bottom nodes around the perimeter of the reflector were removed to further reduce the number of struts and nodes.

The cross sections of the steel struts in the original Leighton BUS were selected to minimize the deviation from homology. The modified BUS for the new design uses the same 13 cm^2 cross-section carbon fiber reinforced plastic (CFRP) tubing for all of the struts. CFRP has a low thermal expansion coefficient and high elastic modulus to weight ratio. The nodes are steel and have an effective length of 10% of the strut length . This gives a very homogenous and isotropic structure.

The gravity deformations of the BUS for different support configurations were calculated using a finite element analysis program [6]. Typically, the configurations had six support points at a radius near 2/3 of the reflector radius. (The original Leighton BUS is supported at 9 nodes at a radius of ~0.33 of the primary radius.) Additional struts connect the support points to the nearby nodes. The radius of the support ring could then be varied without altering the spaceframe. Despite the coarseness of the spaceframe grid, the deformations showed a sharp minimum at 3.43 m, in close agreement with the analytical calculations for a uniform disk. The analytical uniform disk model proved to be a good starting point for evaluating the merits of different support configurations.

A spaceframe BUS avoids the concentration of nodes, struts and forces near the reflector vertex that is common to standard radial rib structures. A large volume near the vertex can be provided for mounting the receiver equipment without jeopardizing the BUS performance. Another advantage of the uniform spaceframe approach is that all of the struts are close to the same length. This makes it relatively easy to tailor the steel nodes and end fitting so that the effective thermal expansion coefficients of all the struts are the same.

B. Elevation Tipping Structure

Supporting the BUS at a large radius improves its performance but also places a large burden on the supporting structure. Distortions in the large ring of supports imprint directly onto the reflector surface. Minimizing the surface errors requires that the support points remain in a flat uniform round ring under gravitational, wind and thermal distortions. One method to achieve this is to use a deep cone to provide a stiff homologous support of the BUS for loads along the optical axis. This type of structure is used on the JCMT and Efflesberg telescopes [4]. Fig. 3 shows the details of the elevation tipping structure that supports the BUS. Six CFRP rods start from a common apex on the rim of the 2.9 m radius elevation drive wheel and extend into the BUS. Six smaller struts at the ends of each of the cone rods connect to the BUS nodes. The apex of the support cone and the elevation wheel are connected to the elevation bearings by a structure of steel beams. There is a large clearance hole in the elevation axis weldment to allow the CFRP cone rod to pass through uninterrupted.

It still remains to provide a structure to resist the transverse loads at the support ring. In the design presented here, this is accomplished using a CFRP latticework from the ring of six support points to the elevation structure as shown in Fig. 3. This latticework keeps the six support points in a circle and transfers the transverse forces from the BUS to the elevation structure. Note that the six primary support points are located inside the spaceframe volume near the plane containing the center of gravity of the BUS. This minimizes the cantilever torsional stress imparted to the BUS when the telescope looks at the horizon or experiences wind forces.

The deep cone rods nicely miss the struts in the backup structure, but the lateral support latticework had to be judiciously arranged to avoid the struts. The latticework is in a plane perpendicular to the optical axis to minimize transference of axial forces from the elevation structure through the latticework to the six support points. The plane of the six primary support points intersects the optical axis above the reflector's vertex. The latticework must be located behind the reflector vertex and ends up 10 cm below the ends of the cone rods.

The thermal properties of this tipping structure are important to the performance of the telescope under the various environmental conditions. The deep cone and latticework are fabricated from low thermal expansion CFRP tubes with cross sections of 25 cm^2 and 6 cm^2. The rest of the structure is fabricated from steel tubes with typical cross sections of 25 cm^2. The thermal expansion of the steel

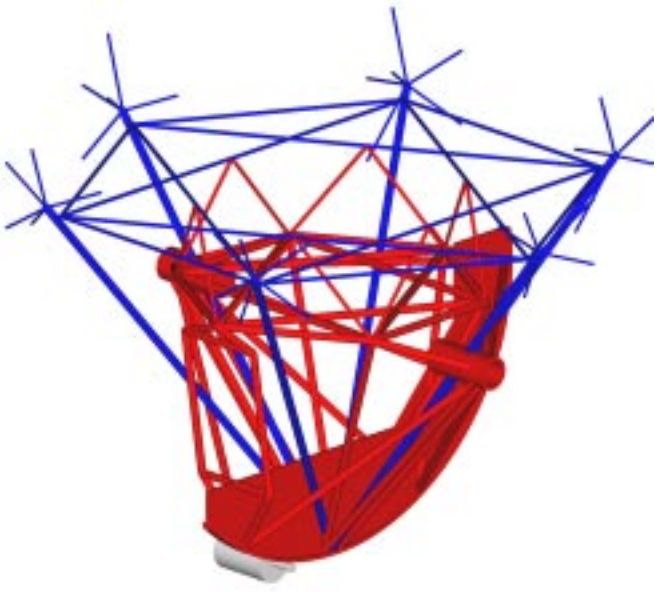

Fig. 3. Basic components of the tipping structure for support of the BUS. The CFRP deep cone for Z-axis support, latticework for lateral support, and connection struts to BUS are shown in blue. The elevation drive wheel and structural steel connection to the elevation bearings are shwn in red. The orientation of this rendering is the same a in Fig. 1.

structure moves the cone apex and deforms the lattice perpendicular to the plane of the latticework, but the six BUS support points remain in a planar circular ring. An alternative to using CFRP tubes for the cone and latticework would be to use steel tubes and regulate their temperature.

There is no active thermal control of the BUS or the tipping structure. The critical parts are CFRP with a coefficient of thermal expansion (CTE) of ~1×10^{-6}/K to minimize effects of temperature gradients. Inclusion of the steel nodes results in an effective CTE of ~2×10^{-6}/K, less than a fifth of steel alone. In addition the BUS and tipping structures are both very open and even light winds will dramatically decrease the thermal gradients [7]. The individual struts and tubes should be painted or have lightweight aluminum foil cladding for UV protection of the CFRP.

The receiver cabin is non-structural and contained inside the volume defined by the support cone and latticework. The steel elevation structure is designed to minimize the encroachment into this volume. The interior cabin volume is hexagonal in shape with a flat to flat distance of 3.2 m at shoulder height, narrowing to 1.8 m at the floor. The minimum height is 1.9 m with a cone extending another 1 m to the reflector vertex.

This design has the usual bilateral symmetry with the azimuth and elevation axes intersecting. It is also easy to balance by adding weight along the rim of the elevation drive wheel. It requires very little counterbalance weight because the elevation axis is close to the reflector vertex and the receiver cabin and elevation drive wheel counter balance the reflector.

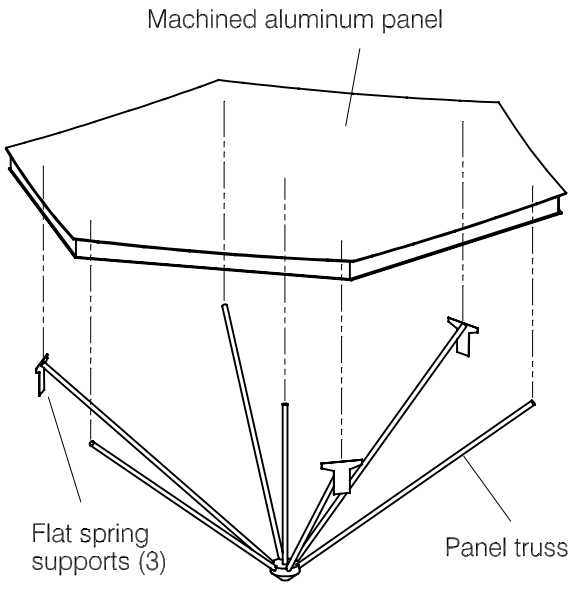

Fig. 4. Reflector panel configuration. The flat springs and the supporting truss are connected behind the front surface of the panel.

C. *Reflector Panels*

The Leighton BUS is designed to support hexagonal panels with a flat-to-flat width of ~1.1 m. These relatively large panels have the advantage of decreasing the BUS complexity and parts count, but the large panels are more difficult to machine and support to meet the surface accuracy requirements. The panel concept used here is based upon the bulk-machined aluminum panels successfully used by Plathner on the IRAM 15-m diameter telescopes [8]. Fig. 4 shows the panel design concept. The panels are ~50 mm thick and milled from aluminum billets. The rear surface of the panel is flat so that the panel is thinner in the center. This gives the best distribution of weight to minimize gravitational distortion. Hexagonal pockets with a distance across the flats of 100 mm are machined into the rear of the panel to leave a lattice of T-shaped ribs. Fig. 5 shows the details of the pockets and rib structure. The front surface and the top of the 'T' on the ribs are 2.5 mm thick and the ribs are 1.5 mm. Rectangular cavities were found to be slightly stiffer but the increase in mass due to the extra material in the corners adds significantly to the panel mass. Furthermore the hexagonal pockets are better suited to the panel shape and give symmetric deflections when the adjustments are applied to the shape at the corners.

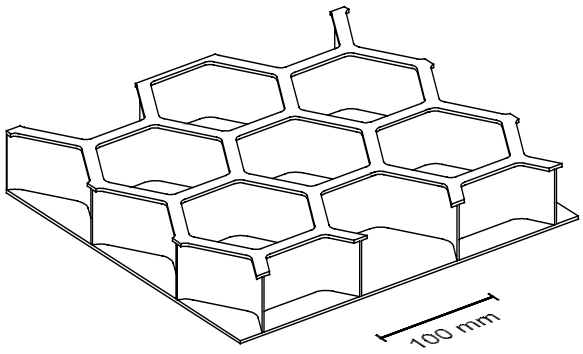

Fig. 5. Section through a panel viewed from the rear showing the T-section ribs.

The panel is supported on three flat springs at alternate corners of the hexagon. The faces of the springs are towards the center of the panel so that differential thermal expansion between the panels and the BUS is taken up with little stress on the panel [9]. However, they still provide good stiffness against lateral forces such as gravity in the horizon pointing direction.

Seven aluminum struts (100 mm^2 cross-section) from the six corners and the center of the panel meet at an apex ~0.7 m behind the panel to increase the panel stiffness. CFRP struts of the same cross-section give a slightly stiffer support, but the deflection due to thermal gradients is nearly identical to that with aluminum struts.

Adjustment of the lengths of the struts allows local deformation at the corners and center to optimize the large-scale figure of the panel. This relieves the requirements on machining such a large area to an absolute accuracy so that machining tolerances need be maintained over distances of only 0.5 m or so. Once the struts are adjusted to optimize the panel shape the three flat spring supports are used to set the panels on the BUS without altering their shape. The thermal properties of the struts may be tailored to compensate for the thermal expansion of the aluminum panels relative to the BUS. A disadvantage of the struts is that three of them need to be removed to mount the panel on the BUS, since they link with the BUS struts. These panels, including the rear truss, have an effective areal mass density of ~13 kg/m^2.

To avoid concentration of heating on the secondary mirror, the surface needs to be cut with a sharp tool. This will result in grooves with a triangular cross-section. In order not to affect the sub-millimeter performance, groove pitch should be less than a wavelength at the highest observing frequency (300 μm). At optical and infrared wavelengths, the grooves will strongly scatter the radiation over an angle of $\geq 20°$ if slope of the groove walls is $\geq 10°$. This applies to the secondary also.

D. *Secondary Mirror and Support*

The mirror is turned from aluminum with ribs on the rear, similar to the panels. A mechanism is provided to translate the secondary position in three directions for focus correction and tracking gravitational changes in the focal point position.

It is supported on a tripod that attaches to the BUS midway between pairs of the six primary support points. This distributes the tripod forces equally to the six points and preserves the homology of the deep cone support. The lowest

resonant frequency of a secondary supporting structure is usually limited by the self-resonant frequency of the individual legs. Hence the legs must each be constructed to have a high resonant frequency. In this case a tripod minimizes the optical blockage. Putting a knee in the feedleg, as shown in Fig. 1, also reduces the optical blockage. This decreases the cross section seen by the spherical wave centered on the prime focus [10]. The tripod legs are to be fabricated from high modulus CFRP material with a sheet thickness of 3 mm. They have a width of 50 mm in the aperture plane and a depth of ~0.2 m. The 0.61 m diameter secondary and its mechanisms are assumed to weigh 50 kg.

The optical blockage for this design is 0.34% from the secondary, 0.41% for the plane wave tripod blockage, plus 1.68% for the spherical wave component for a total of 2.43%. These values assume no taper in the aperture illumination. With a 12-dB taper the total effective area blockage is 2.57%.

III. Mount

The mount is an important part of the telescope since the lowest resonant frequency for the whole structure is usually limited by mount stiffness. Fig. 1 shows the major structural features. The rotating azimuth structure is constructed from 6500 mm^2 cross section steel pipe. The azimuth bearing is a 5.1 m diameter wheel and track system with a central pintle bearing. A wheel and track bearing can have a very high stiffness with low friction. The wheels and track are enclosed with a sliding seal to avoid contamination from wind blown dust and dirt. The base is a 1.1 m high cylinder with the azimuth track attached to the top. This provides a very stiff mount and pushes the resonant frequency of the structure above 10 Hz.

A. Base

The base is attached to the foundation at eight points. It would be very difficult to achieve the desired high stiffness and resonant frequency with only three attachment points. It is important that the eight points carry equal loads and that the track at the top of the base remain flat. This can be achieved by manufacturing the base with a precise depth from the top of the track to the interface with the foundation and adjusting the top of the eight attachment points on the foundation to lie in a level plane. The adjustment of the foundation attachment points to a level plane would be done after construction. This might be as simple as using threaded studs in the foundation with large diameter lockable nuts for the mount to rest on. Surveying the tops of these nuts would ensure they all lay on a horizontal plane to the desired precision. No adjustments of the base or the foundations should be required for routine moving and setting of the antennas. This general strategy is applicable to mounts with four or more attachment points.

The mount configuration also gives a large tracking range for the telescope. It can operate clear down to the horizon at 0° elevation and also past the zenith to an elevation of 120°. These features may be useful for measuring and setting the surface. The mount design in combination with the short distance from the reflector vertex to the elevation axis gives a very small swept volume for the telescope for full sky tracking. Two 10.4 m diameter telescopes can be placed 12.1 m apart without any possibility of collision. This gives a very small close packing limit of 1.16*D*.

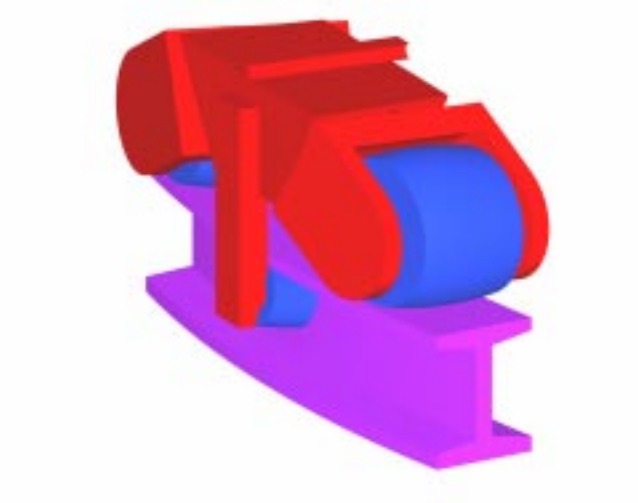

Fig. 6. Schematic of azimuth track with auto-tracking bogies.

B. Drive System

Meeting the fast position switching requirement will require an advanced control system. The design of the control system will require a detailed servo analysis based on a complete FEA of the telescope structure that is beyond the scope of this paper. It is clear, however, that the drive components should be stiff enough to not significantly limit the locked rotor resonant frequency and should have minimum backlash.

It is anticipated that the elevation friction drive will use a torque motor with a 50-100 mm diameter pinion shaft in high-pressure contact with the elevation drive wheel. The choice of the pinion shaft diameter will be a compromise between the desired drive reduction ratio and the effective torsional stiffness [11]. A detailed servo analysis is required to determine the optimal shaft diameter along with many other servo parameters.

The azimuth wheel bogies use an auto-tracking configuration, shown in Fig. 6, with barrel shaped rollers to avoid the accumulated strain and sudden release that can occur in straight cone wheels [12]. Fig. 6 also shows the carriage wheels that hold the base to the rotating azimuth structure when the telescope is picked up and moved. The azimuth wheels will be directly coupled to the drive motors. Four or even all eight of the azimuth wheels can have drive motors.

IV. Pointing Reference Structure

One of the important scientific goals for the MMA is high fidelity maps of fields much larger than size of the primary

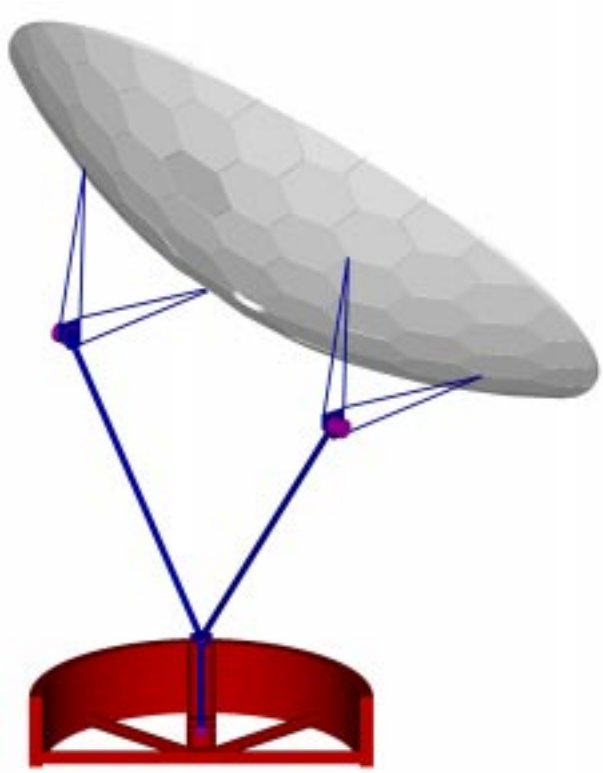

Fig. 7. Independent pointing reference structure. The CFRP beams are shown in blue and the encoders are magenta. The steel base is shown in red.

beam. This requires combining data from many pointings of the telescope with an accuracy of $1/30^{th}$ of the primary beam, much tighter than the usual pointing specifications of radio telescopes. This translates to pointing accuracy of 0.8 arcsec for a 10 m diameter telescope operating at a wavelength of 1 mm, presenting a difficult design challenge. The required pointing accuracy under most environmental conditions is significantly better than achieved on current telescopes but is not beyond what can be expected from a carefully designed structure utilizing modern materials.

There is extensive pointing experience with the Leighton telescopes in operation at the Owens Valley Radio Observatory (OVRO) and at the Caltech Sub-millimeter Observatory (CSO) on the top of Mauna Kea in Hawaii. These telescope a blind pointing accuracy better than 4 arcsec at night and better than 6 arcsec during the day. Environmentally induced distortion of the structure is responsible for most of the pointing error. In particular, thermal distortions of the BUS and mount can account for a large fraction of the pointing error [7]. The telescopes use tiltmeters mounted on the axis of the rotating azimuth structure to correct for the tilting of the azimuth axis in real-time. This additional metrology is crucial to correcting for distortions in the mount. The tiltmeters along with shielding the elevation yokes from the sunlight were found to be necessary for good pointing performance.

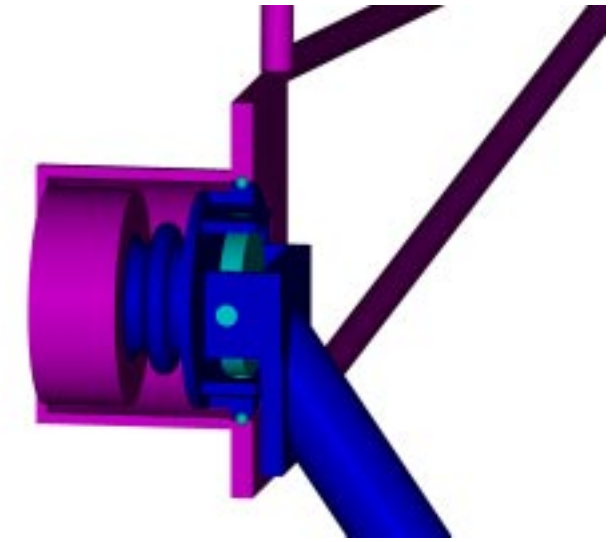

Fig. 8. Details of the elevation encoder mounting. The structure connected to the reflector nodes, including the encoder body is shown in magenta. The structure shown in blue is part of the azimuth reference arm, including the coupler to the encoder.

A. Elevation and Azimuth Encoders

The approach taken in the new telescope design presented here is to use an independent reference structure for the pointing system. Fig. 7 shows the pointing reference structure (PRS) and encoder configuration. It measures the position and orientation of four representative nodes on the reflector surface relative to the telescope foundation. This structure does not carry any structural loads and is thermally stable. Standard encoders measure the elevation and azimuth orientation of the reflector.

The elevation encoders at the “elbows” measure the rotation angle of the reflector relative to the azimuth reference arms. Two elevation encoders are used to provide a symmetrical arrangement and provide information about possible twisting of the reflector. The elevation encoders are positioned on the elevation axis but are separate from the actual elevation axle and bearings. Special care is taken in providing a housing and support bearing for the elevation encoders to avoid transferring even the light gravity load from the weight of the azimuth arms to the encoder’s internal bearings. Fig. 8 shows a cutaway view of an elevation encoder mounting.

The azimuth reference arms are connected to a hub on the azimuth reference axle. Fig. 9 shows the details of the azimuth reference structure. As the telescope rotates, the motion of the reflector is transferred to the two azimuth arms via the two elevation encoder housing bearings and hence to the azimuth axle. The encoder at the bottom of the axle measures the rotation of this axle. The stationary half of the azimuth encoder is attached to the bottom circumference of the mount base independently of the pintle bearing.

The elevation and azimuth encoders give the orientation information normally measured in an alt-az mount but

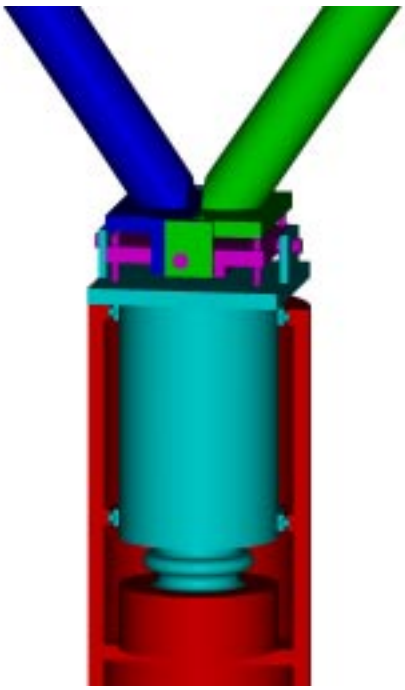

Fig. 9. Details of azimuth axle section of the pointing reference structure. The left and right reference arms are shown in blue and green respectively. They are independent but share a common axle in the gimbal, shown in purple. The azimuth reference axle is light blue, while the fixed encoder body and base housing are red. The gap sensors are the narrow vertical cylinders on the purple gimbal plate.

without the errors caused by the mount distortions. Using low CTE CFRP for the beams in the reference structure minimizes the environmental effects. The azimuth reference arms are shielded from wind and sun by the azimuth structure enclosure.

It is necessary to provide compliance in the reference structure to accommodate the distortions in the mount and elevation structure without jeopardizing the accuracy and stability of the encoder readings. The elevation arms are free to rotate about the line connecting the pair of reflector nodes they are connected to and there are gimbals at both ends of the azimuth arms. The range of motion at these points is very small (less than an arcminute) and bearings are not required. Fig. 10 shows a design concept for flex-pivots that could be used in place of bearings. These flex-pivots have no "moving" parts and provide high translation rigidity with low torsion stiffness over very small angular ranges.

Fig. 10. Flex-pivot with high translation rigidity and low torsion stiffness for very small angles.

B. Additional Metrology

Additional information is provided by the tiltmeter and gap sensors mounted on the azimuth gimbal plate. During normal tracking, the tiltmeter gives a reference to the local gravity and can be added to the elevation encoder reading to give the "true" elevation orientation of the reflector independent of distortions in the elevation and azimuth structures. The gap sensors are used as precision angle encoders over a small range. The sensors on the azimuth arms measure the elevation angle of the azimuth arms relative to the hub. These angles plus the known length of the arms and tiltmeter readings precisely determine the location of the elevation encoders. This provides a measure of the cross-axis tilt of the effective elevation axis, a quantity that is not normally measured on elevation over azimuth mounts. The extra metrology utilizes proven technology and is confined to a small volume in the base of the telescope around the azimuth axis where the temperature can be accurately regulated.

The azimuth arm elevation angles will be a function of the reflector elevation if the encoder housing bearings are not aligned with the mount elevation bearings. The system is tolerant of small errors in this alignment and the arm angle variation can be used to verify that the system is within specification.

Tiltmeters must be mounted very close to the azimuth axis to prevent centripetal accelerations from affecting the readings. Careful mounting of the gimbal plate tiltmeter will give negligible errors for normal sidereal tracking away from the zenith, but the errors may be large during the fast position switching trajectories. Gap sensors between the gimbal plate and the azimuth axle are used to supplement the tiltmeter readings during fast rotations or accelerations. An auxiliary tiltmeter attached to the base near the encoder determines the tilt of the azimuth axle housing.

The gap sensors must have an accuracy of ~0.1 μm but the range is only ~100 μm. The dynamic range is small and several sensor technologies can satisfy these requirements. Twice as many sensors are shown in Fig. 9 as are actually needed. This redundant information will help ascertain how well the system is performing and aid in locating possible problems.

Although this pointing system looks quite different from the traditional elevation over azimuth encoder system, it is functionally very similar. In particular the system will work as well as or better that the traditional system without the tiltmeters and gap sensors. The extra metrology augments the encoders to provide the additional information necessary to correct for deformations of the mount and elevation structure. The reference structure and metrology could be implemented piecemeal around the traditional encoder configurations, but

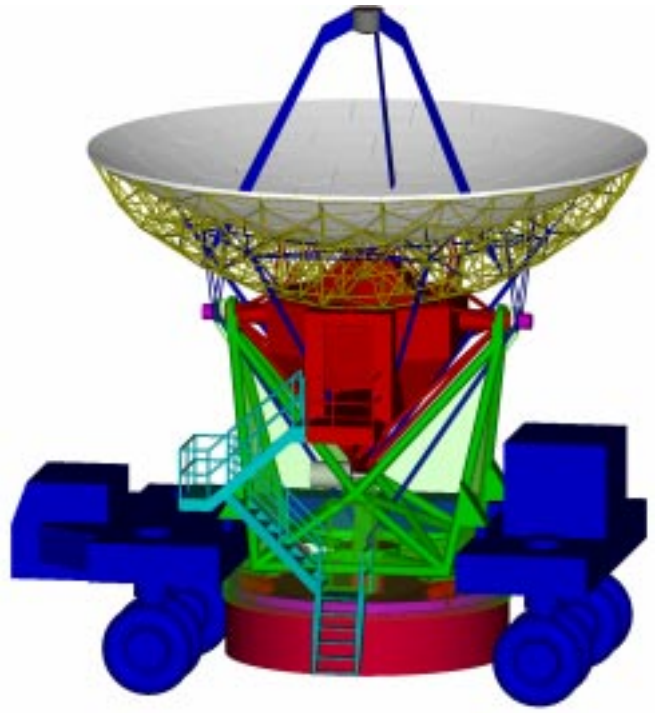

Fig. 11. Design sketch for telescope transporter. The driver's cabin is on the left and the power plant is on the right

we were interested in exploring a more fundamental approach to the difficult problem of meeting the stringent pointing specifications for the MMA antennas.

With these improvements it is no longer necessary to put the full burden of the pointing specification on the passive mount. The tiltmeters define an effective azimuth axis parallel to local gravity and the azimuth bearing does not have to be perfectly level or flat. The mount must have a high resonant frequency and smooth tracking to allow the servo control system to function properly. This in turn requires high stiffness and low or at least constant friction. The mount described in the previous section has these properties.

V. Transporter

The MMA is a reconfigurable array and the telescopes must be easily transported between foundation pads. The large diameter of the base requires an innovative design for transporter that will move the telescopes. A possible solution is sketched in Fig. 11. It uses four pairs of wheels that can be steered in any direction. The transporter frame is in a "C" shape to allow it to straddle the telescope by moving sideways. Hydraulic pistons then rise to lift the telescope off the foundation. The pistons are controlled to maintain the telescope in a level unstressed condition during transit over uneven terrain. The four pairs of wheels contain independent motors and a sophisticated control system will be required to coordinate the steering and drive power to all of the wheels.

The outside wheel width of the transporter is 6 m. This width greatly improves the stability for carrying the telescope over rough ground. Even so it is narrow enough to drive between two telescopes that are spaced at the minimum allowable 1.16*D* spacing. It also fits on the Atacama international highway, albeit with traffic blocked in both directions.

The process of setting an antenna onto a foundation pad should be as simple as possible to allow rapid reconfiguration of the array and to avoid mistakes. The foundations will have two protruding pins that match a hole and a slot on the telescopes to provide kinematic azimuthal alignment when setting the antenna down on a pad. The antennas will have a remotely operated clamp system to firmly attach the base to the eight attachment points in the foundation. It is anticipated that all operations required to move a telescope from one pad to another (with the possible exception of electrical connections) would be done from the transporters cabin using television cameras to monitor all of the steps. The cabin will

TABLE I: Bill of Materials for Telescope with Weight Budget

Item	**Material**	**Quantity**	**Mass [kg]**
Tipping structure			
Mirror	Aluminum	1 hyperbola	6
Mechanism	Steel	3-axis control	40
Feedlegs	CFRP, high mod.	3 legs	34
Surface panels	Bulk machined Al	85 panels	1,100
Panel stiffeners	CFRP, 20×1mm tube	85×7×~1 m	6
Adjusters	Differential screws	99	45
BUS struts	CFRP, 50×4mm tube	749×~0.9 m	657
BUS nodes	Steel	177×2 kg	354
BUS XY trellis	CFRP, 50×4 mm tube	12×4.6 m	67
BUS Z cone	CFRP, 100×8 mm tube	6×6.4 m	159
Elev. structure	Steel, 100×4 mm tube	~40×5 m	2,000
Elevation wheel	Steel ring, 100×50 mm	4.5 m	186
Elev. drive motor	Direct drive pinion	1 or 2?	200
Enclosure & instr.	Al and foam walls	100 m^2	2,000
Counter weight	Bulk steel	0.16 m^3	1,300
		Subtotal	**8,154**
Azimuth structure			
Structural support	Steel, 250×8mm tube	~5m	13,000
Elev. bearings	30 cm dia.	2	200
Central bearing	1 m dia.	1	500
Azimuth wheels	Double bogies	4	4,000
Az. drive motors	Direct drive to wheels	2 or 4	1,000
Enclosure & instr.	Al and foam walls	400 m^2	4,000
		Subtotal	**22,700**
Base structure			
Azimuth track	5 m dia. circular rail	6,500 mm^2	850
Track support	Steel plate, 25 mm	~30 m^2	6,000
		Subtotal	**6,850**
Pointing structure			
El. encod support	CFRP, 50×4 mm tubes	8×~2 m	16
El. encoders	24-bit, incremental	2	100
El. reference arms	CFRP, 150×1 mm tube	2×5 m	8
Gimbals	XY	2-axis	10
Tiltmeters	Electrolytic bubble	2-axis	2
Gap sensors	1 mm ran., 1 μm prec.	4	2
Azimuth bearings	Precision 10 cm dia.	2	10
Azimuth encoder	24-bit, incremental	1	50
Base tiltmeters	Electrolytic bubble	2-axis	2
		Subtotal	**200**
		Total	**37,900**

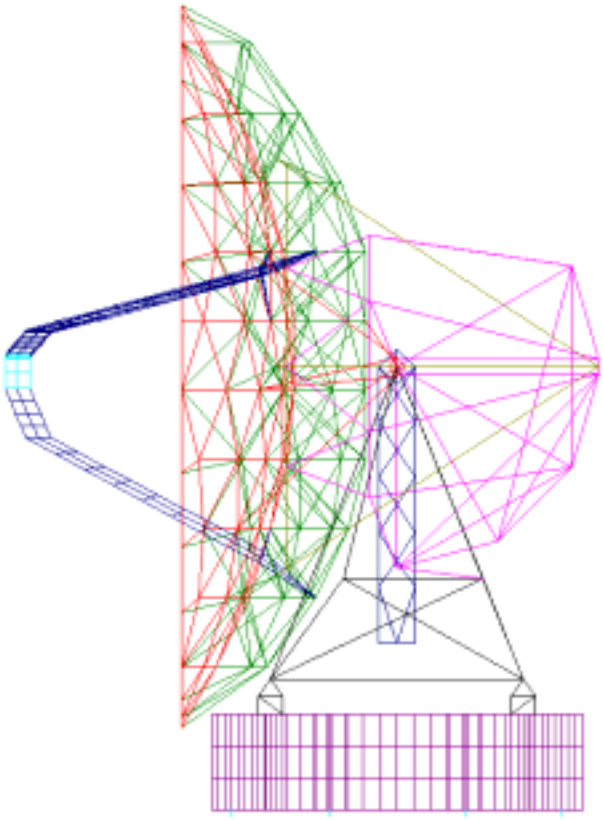

Fig. 12. Wire frame model used in ALGOR analysis of the telescope.

be oxygen enriched to avoid the debilitating effects of the 5,000 m elevation at the MMA Atacama site.

VI. Performance Calculations

The major components in this design have been combined into a finite element model, FEM, of the complete structure. The physical configuration was generated using AutoCAD R14 [13] and the .DXF files were used to generate the geometry in ALGOR [6]. The model consists of 2,700 plate and beam elements connected at 1,500 nodes. Table I lists the bill of materials for the telescope and indicates the quantity and types of material used in the model. The level of detail in the model is indicated in the ALGOR wire frame drawing of the model shown in Fig. 12.

The model was then subjected to a variety of loads to represent the environmental conditions the telescope is expected to experience during operation. The loads included gravity, temperature and wind. A C-program was written that would operate on the ALGOR element input files to impose a variety of temperature distributions on the structure before analysis. Wind forces were approximated by applying forces on the reflector surface nodes. The total wind force was estimated using reasonable drag coefficients and this total force was evenly distributed among all of the surface nodes.

The output from the ALGOR analysis was read into a Mathcad [14] program that used the node displacements to

Summary of results file = "gravity_zenith.txt"

Structural calculation results using the primary senors with no corrections.

Quantity	Transducer measurements		Error (actual - measured)
Path length	Spath = 493.5 μm		patherr = −2.1 μm
Elevation pointing	elencoder = 0.7 arcsec	tilt = −0.8 arcsec	$\delta\phi_x$ = 0.6 arcsec
Azimuth pointing	azencoder = −0.0 arcsec	cross0 = 0.0 arcsec	$\delta\phi_y$ = 0.0 arcsec
Net pointing error			pointerr = 0.6 arcsec
RMS surface error			RMSafterpnt = 15.2 μm
RMS surface error after optimizing secondary position			bestfitRMS = 9.5 μm

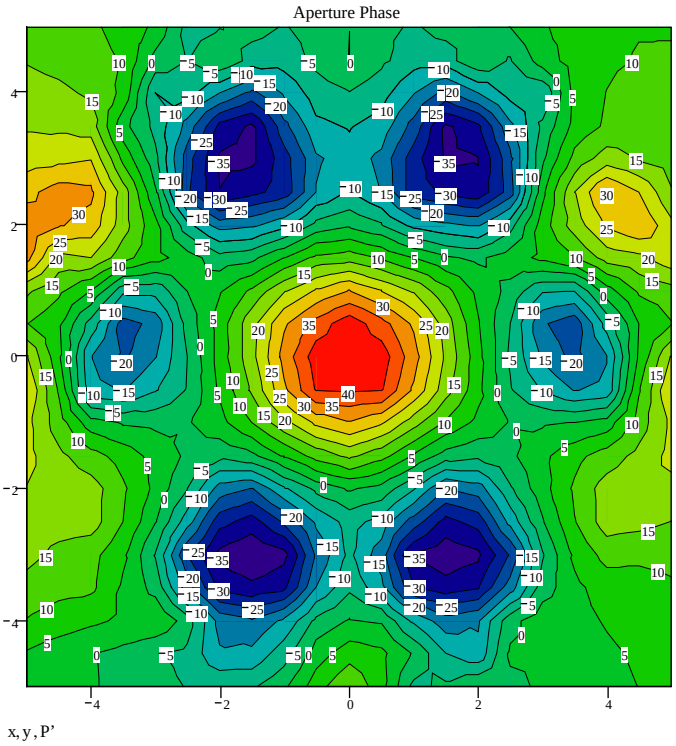

Fig. 13. Output from Mathcad analysis program with contour map for the wave front error in microns.

calculate the quantities of interest. The most important performance parameters are the wave front, pointing, and path length errors. The surface nodes, back focal point of the secondary, receiver mount location, and representative elements in the PRS were tracked. The Mathcad program calculates the net wave front distortions for the whole optical system from the receiver mounting point to the nominal aperture plane.

Fig. 13 shows an example of the output from the Mathcad program for the vertical gravity case. The pointing and path length changes measured by the metrology is summarized along with the final difference between the "measured" and actual value of these parameters. The peak-to-peak wave front error (WFE) is only 100 μm before optimizing the secondary position. This corresponds ~50 μm peak-to-peak surface displacement and is indicative of the high stiffness of a spaceframe supported at a large radius. The contour plot in Fig. 13 shows the WFE after shifting the secondary by 134

TABLE II: . FINITE ELEMENT ANALYSIS SUMMARY FOR REPRESENTATIVE LOAD CASES.

Case	Path Change	Path Error	Pointing Change	Pointing Error	½ WFE	½ WFE after fit
1 Gravity, zenith	494.0	-2.1	0.5	0.6	15.2	9.5
2 Gravity, horizon	-11.1	-7.2	9.1	16.2	21.5	7.2
3 Wind, zen., X-axis	0.0	0.0	0.6	0.1	0.3	0.1
4 Wind, zen., Y-axis	0.1	0.0	1.1	0.1	0.3	0.1
5 Wind, hor., X axis	0.0	0.0	0.3	0.3	0.5	0.2
6 Wind, hor., Z axis	81.2	3.3	2.7	0.0	3.7	1.2
7 Temp., zen., uniform 10 C	-348.0	-29.0	0.0	0.3	6.0	0.7
8 Temp., hor., uniform 10 C	382.0	-15.1	8.3	0.0	6.3	2.0
9 Temp., hor., dT/dX=1C/m	0.0	0.0	1.0	0.1	0.4	0.3
10 Temp., hor., dT/dY=1C/m	93.3	-4.0	0.7	0.4	5.0	0.5
11 Temp., hor., $T(R)=.2R[m]^2$	111.0	-3.9	2.2	0.0	5.0	0.4
12 Temp., zen., meas. [7]	2.2	0.7	1.1	0.1	1.5	0.6

μm in the Z-direction to minimize the WFE. The residual effective surface error is 9.5 μm RMS for this load case.

A summary of the load conditions analyzed and the resulting performance are given in Table II. The performance was calculated using a total system approach. The average wave front phase is the path length change given in column 2. The displacements of the elements in the PRS are used to determine what the encoder, tiltmeter, and gap sensor readings would be. These readings are then used to calculate corrections to the path length and pointing direction of the telescope. These are the same calculations that a real-time computer would make using the encoder and metrology readings. Column 3 in Table II is the path length error after applying the metrology corrections. Similarly column 4 in the tilt to the wave front across the nominal aperture plane, while column 5 is the wave front tilt remaining after applying the calculated encoder and metrology corrections. This residual tilt would show up as a pointing error during operation of the telescope. Half of the RMS residual after removing the best-fit path length and tilt is the effective surface error given in column 6. This calculation uses a uniform aperture illumination. Column 7 is the effective surface error after optimizing the position of the secondary. This last step is analogous to removing the best-fit paraboloid from the surface distortions. All the load cases except the two gravity cases are assumed to be unpredictable and column 6 should be used for calculating the RMS surface error. Load case 12 applies the worst case measured temperatures for the Leighton telescopes operating at OVRO.

The vertical and horizontal gravity load cases are special in that the load is predictable and the secondary can be moved to the optimal position during operation. Hence column 7 is the deviation from homology for gravity. Also the relatively large pointing errors for cases 1 and 2 can be included in the telescope pointing model and are not part of the pointing error budget.

Proper adjustment of the reflector surface can reduce the gravity induced surface errors beyond the values given in column 7 of Table II. The distortions in the telescope surface are linear and elastic, and the distortion at any angle is a linear superposition of the vertical and horizontal distortions. A common procedure is to set the surface to be "perfect" at a selected rigging angle [15] with the errors increasing away from this rigging angle. The peak RMS surface error over the full elevation range can be reduced significantly using a different surface setting strategy [3]. The idea is to subtract half of the sum of the zenith and horizon distortions from the perfect surface in zero gravity. This procedure minimizes the RMS at the extremes of the elevation range. A surface adjusted in this way is not perfect at any angle and it has to be set to a pre-calculated shape at the angle used for the accurate surface measurements. This procedure will yield a surface error at the zenith and horizon equal to the half of the RSS combination of the vertical and horizontal distortions for most structures. The worst case gravity contribution to the surface error budget for this telescope is only 6.0 microns. Reference [3] describes refinements to the tuning procedure that can further improve the surface optimization.

A. Wave Front Error Budget

Many components and load conditions contribute to the wave front error (WFE). Table III is an extensive listing the expected contributions to the ½ WFE for this design. The worst relevant cases from Table II are used for the wind and thermal contributions to the BUS errors. The wind and thermal contributions for the panels and secondary are based on simple modeling of these structures using estimates for the temperature and wind loads. The manufacturing and alignment contributions are based upon experience with similar structures.

B. Pointing Error Budget

Table IV summaries the non-repeatable pointing errors. The repeatable errors should not cause pointing errors since they can be incorporated into the pointing model. The gravity pointing errors are in this category. The gravity contribution in Table IV accounts for possible hysteresis or gaps in the joints of the fabricated structure. The wind and thermal distortions of the PRS are included in the FEA results in Table I, but bearing friction and slop is included as a separate contribution.

The pointing specifications for the MMA antennas provide for astronomical recalibration of the pointing offsets on a nearby point source every 20 minutes. This greatly reduces the effects of drifts in the metrology sensors and removes the effect of bearing or encoder eccentricity. It can be argued that pointing recalibration will also reduce the thermal errors

TABLE III: SURFACE ERROR BUDGET

	Effective surface error [μm]
Backing structure	
Gravity (ideal)	6
Gravity (departure from ideal)	3
Absolute temperature	6
Temperature gradient	5
Wind	4
Subtotal	**11.0**
Panel and supports	
Manufacturing	10
Absolute temperature	4
Temperature gradient	4
Gravity	5
Wind	5
Aging	3
Panel location in plane	2
Panel adjustment perpendicular to plane	3
Subtotal	**14.0**
Secondary mirror	
Manufacturing	5
Absolute temperature	2
Temperature gradient	2
Gravity	2
Wind	2
Aging	2
Alignment	5
Subtotal	**8.4**
Surface setting (holography)	
all contributions	10
Subtotal	**10.0**
Total (rss)	**22.1**

and even some of the wind errors, but no such reduction of these errors is applied to the contributions in Table IV.

C. Resonant Frequency

An important aspect of this telescope design is achieving a high resonant frequency. This will make it much easier to meet the fast position switching requirement. The very stiff spaceframe BUS supported at a large radius and the large diameter wheel and track azimuth bearing make it possible to keep the lowest eigenmode well above 10 Hz.

The CFRP BUS plus reflector has a lowest resonant frequency of 48 Hz. The feedlegs are long thin beams and even with high-modulus CFRP and the self-resonance for an individual leg is only 21 Hz. This frequency can be increased, but at the cost of increased aperture blockage. The resonant frequency for the whole tipping structure shown in Fig. 3 plus the primary and secondary reflectors is 16 Hz.

The first three eigenmodes for the whole telescope structure are gross bending or twisting modes about the three principle axes. Fig. 14 shows the lowest eigenmode. This mode has a frequency of 13.5 Hz while the next two modes are at 14.3 and 14.8 Hz. The next lowest mode is at 19.7 Hz. These resonances are consistent with the expected best achievable for a telescope of this diameter [2] and should be sufficient for implementing a servo system capable of meeting the fast position switching requirement. If these

TABLE IV: POINTING ERROR BUDGET

	Pointing error [arcsec]
Gravity (departure from ideal)	0.1
Wind	0.3
Absolute temperature	0.3
Temperature gradient	0.4
Encoders (24-bit)	0.1
Metrology (tiltmeters and gap sensors)	0.1
Reference structure (bearing slop and friction)	0.1
Total	**0.6**

frequencies are higher than required, the weight of the mount and base can be reduced significantly.

VII. SUMMARY

A telescope design that meets the stringent requirements for the MMA antennas has been presented. The effective surface error is 22 μm, the pointing precision is 0.6 arcsec and the lowest resonant frequency is 13.5 Hz. Although the cassegrain elevation over azimuth configuration is conventional, several different design concepts are combined to achieve the excellent performance.

The BUS is a modified version of the triangular spaceframe used for the Leighton 10.4-m telescopes [3]. It is supported at six points in a ring with a diameter of 0.67 of the reflector diameter. The six points are connected to the

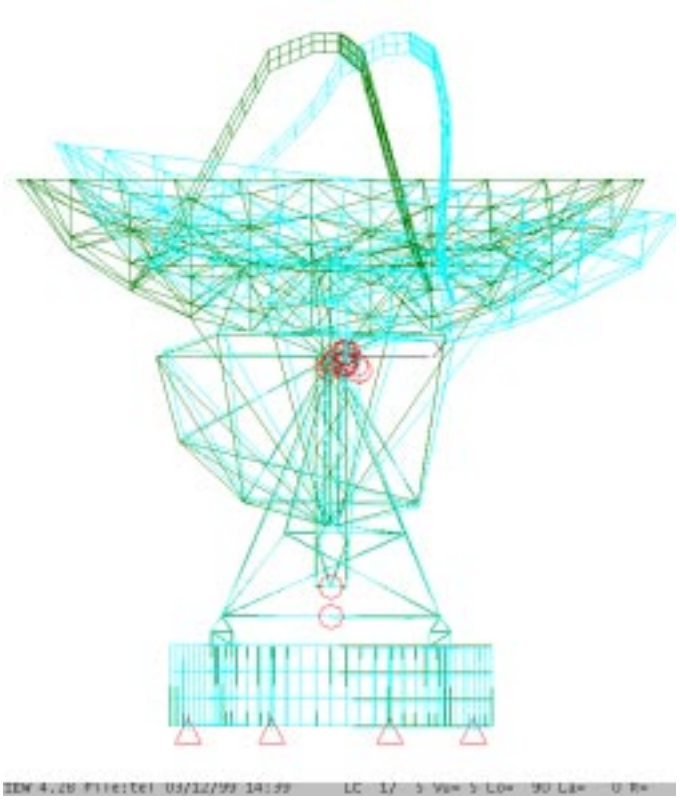

Fig. 14. Lowest eigenmode for the telescope structure. This mode has a frequency of 13.5 Hz.

elevation tipping structure by a deep cone of six rods for axial loads plus a latticework for kinematic transfer of the lateral loads. The large diameter support of the BUS plays an important role in the excellent surface accuracy and high resonant frequency. The BUS, cone rods and latticework are use CFRP for its excellent strength to weight ratio and low CTE.

The Leighton reflector has only 84 hexagonal panels. The fewer large panels simplifies the BUS fabrication compared to the standard rings of pie shaped panels at the cost of a more complex panel design. The panels are machined out of bulk aluminum with an added cone of struts to provide additional stiffness and compensate for gravity and thermal distortion.

A CFRP tripod supports the secondary. The tripod in attached at the same 0.67 of the dish diameter as the six primary supports. This gives excellent mechanical performance while the tripod leg configuration is designed to minimize the optical blockage. The total blockage is only 2.4% most of which can be reflected onto the cold sky to minimize its contribution to the system temperature.

A fundamental improvement in the pointing performance compared to existing radio telescopes is achieved by implementing a separate pointing reference structure. This structure does not carry any structural loads and is designed to unambiguously measure the “true” pointing orientation of the telescope. In addition to the usual elevation and azimuth encoders, it has tiltmeters and gap sensors to refine the pointing precision. This system also measures the cross-axis pointing error, a quantity that is not available in conventional configurations.

The mount has high stiffness without excessive weight. The independent pointing structure offers the advantage that the accuracy and flatness of the azimuth bearing does not directly affect the pointing accuracy. This design utilizes a very stiff large diameter wheel and track azimuth bearing. The track sits atop a 1.1 m deep cylinder that is attached to the foundation at eight points to provide a rigid base. A simple fully triangulated steel beam rotating azimuth structure maintains the mount stiffness to the elevation axis. The large diameter base requires a fairly large transporter to move the antenna between foundation pads, but a viable design concept has been presented.

The performance calculations given in this paper are based on modeling the whole telescope structure using a FEA package. Another program was used to analyze the distortions and evaluate the WFE for the optical path from the sky to the receiver. This program also evaluated the ability of the independent reference system to measure and correct for pointing and path length errors.

This is a conceptual design with enough detail to understand the major performance parameters. The design has not been fully optimized and significant improvement may be possible. A much more detailed design is required to fully evaluate how a telescope that uses these concepts will perform. The model will continue to be refined as the design progresses towards realization. Additional load cases of interest will also be analyzed in the near future.

ACKNOWLEDGEMENTS

The work presented here is the result of discussions with many people, especially the NRAO MMA Antenna Working Group consisting of J. Bieging, J. Cheng, D. Emerson, M. Fleming, M. Holdaway, J. Kingsley, J. Lugten, J. Mangum, P. Napier and, W. Welch.

We would also like to think Dietmar Plathner for inspiring us in the direction this design has taken.

REFERENCES

[1] D. Plathner, "A next generation radiotelescope of the 12 to 15 m class for the future large interferometer arrays in the southern hemisphere," Proc. SPIE vol. 3357, *Advanced Technology MMW, Radio, and Tereahertz Telescopes*, ed. T. G. Phillips, 1998 pp. 755-762, 1998.

[2] S. von Hoerner, "Design of large steerable antennas," *Astron. J.*, vol. 72, pp. 35-47, 1967.
S. von Hoerner and Woon-Yin Wong, "Gravitational deformations and astigmatism of tiltable radio telescopes," *IEEE Trans. Ant and Prop.*, pp. 689-695, September, 1975.

[3] D. Woody, E. Serabyn and A. Schinckel, "Measurement, modeling and adjustment of the 10.4 m diameter Leighton telescopes," Proc. SPIE vol. 3357, *Advanced Technology MMW, Radio, and Tereahertz Telescopes*, ed. T. G. Phillips, 1998 pp. 474-484, 1998.
David Woody, David Vail, and Walter Schaal, "Design, construction, and performance of the Leighton 10.4-m diameter radio telescopes," *Proc. IEEE*, vol. 82, pp. 673-686, 1994.

[4] O. Hachenberg, "The new Bonn 100-Meter radio telescope," *Sky and Telescope*, pp. 338-343, December, 1970.

[5] L. A. Selke, "Theoretical elastic deflections of a thick horizontal circular mirror on a ring support," *Applied Optics*, vol. 9, pp. 149-153 Jan. 1970.

[6] Algor: Algor, Inc., 150 Beta Drive, Pittsburgh, PA 15238-2932 USA

[7] J. W. Lamb and D. P. Woody: “Thermal behavior of the Leighton 10-m antenna backing structure,” *NRAO Millimeter Array Memo Series*, No. 234, October 1998.

[8] D. Plathner: “Progress report on aluminium panels,” *IRAM Working Report No. 224/94*, 1994.

[9] R. E. Hills, J. W. Lamb and A. D. Olver: “United Kingdom/ Netherlands Millimetrewave Telescope Antenna,” *Proc. Int. Symp. Antennas and Propagat.*, pp. 955-958, Kyoto, Japan, August 1985.

[10] J. Ruze, “Feed support blockage loss in parabolic antennas,” *Microwave J.*, vol. 11, no. 12, pp. 76–80,1968.

[11] M. Fleming memo on drive systems, in process.

[12] H. McGinness, "Lateral and drag forces on misaligned cylindrical rollers," TDA Progress Report 42-69, Jet Propoulsion Laboratory, Pasadena, CA, pp. 174-178, March and April 1982.
Fred Sills, "Stiction Talks," Brevard Technical Journal, vol. pp31-36, 1992.

[13] AutoCAD R14: Autodesk, Inc., 111 McInnis, Parkway,San Rafael, California 94903, USA

[14] Mathcad: MathSoft, Inc. 101 Main Street, Cambridge, MA 02142-1521.

[15] R. Levy, “A Method for Selecting Antenna Rigging Angles to Improve Performance,” *The Deep Space Network*, Space Programs Summary 37-65, vol. II, Jet Propulsion Laboratory, Pasadena., pp. 72-76, 1970.